Key Points:

- Lunar dust simulants chemically reduced to mimic "space weathering" by solar wind were more toxic than the non-reduced materials
- New probes were employed to assess mitochondrial function, real-time O_2 consumption, and nuclear DNA damage
- Antioxidant supplementation of the cells decreased all the toxic endpoints examined, showing a key role for free radicals in the toxicity

Correspondence to:
B. Demple,
bruce.demple@stonybrook.edu

Author Contributions:
Conceptualization: J. A. Hurowitz, H. Nekvasil, B. Demple
Data curation: J. H. M. Chang, Z. Xue, J. Bauer, D. A. Hendrix, T. Catalano
Formal analysis: J. H. M. Chang, Z. Xue, J. Bauer, B. Wehle, D. A. Hendrix, T. Catalano, J. A. Hurowitz, H. Nekvasil, B. Demple
Funding acquisition: J. A. Hurowitz, H. Nekvasil, B. Demple
Investigation: J. H. M. Chang, Z. Xue, J. Bauer, B. Wehle, D. A. Hendrix, T. Catalano
Methodology: J. H. M. Chang, Z. Xue, J. Bauer, B. Wehle, D. A. Hendrix, T. Catalano, B. Demple

Artificial Space Weathering to Mimic Solar Wind Enhances the Toxicity of Lunar Dust Simulants in Human Lung Cells

J. H. M. Chang[1] , **Z. Xue[1]**, **J. Bauer[1]** , **B. Wehle[1]** , **D. A. Hendrix[2,3]** , **T. Catalano[2]**, **J. A. Hurowitz[2]** , **H. Nekvasil[2]** , and **B. Demple[4]**

[1]Department of Pharmacological Sciences, Renaissance School of Medicine, Stony Brook University, Stony Brook, NY, USA, [2]Department of Geosciences, Stony Brook University, Stony Brook, NY, USA, [3]National High Magnetic Field Laboratory, Florida State University, Tallahassee, FL, USA, [4]Departments of Pharmacological Sciences and of Radiation Oncology, Renaissance School of Medicine, Stony Brook University, Stony Brook, NY, USA

Abstract During NASA's Apollo missions, inhalation of dust particles from lunar regolith was identified as a potential occupational hazard for astronauts. These fine particles adhered tightly to spacesuits and were unavoidably brought into the living areas of the spacecraft. Apollo astronauts reported that exposure to the dust caused intense respiratory and ocular irritation. This problem is a potential challenge for the Artemis Program, which aims to return humans to the Moon for extended stays in this decade. Since lunar dust is "weathered" by space radiation, solar wind, and the incessant bombardment of micrometeorites, we investigated whether treatment of lunar regolith simulants to mimic space weathering enhanced their toxicity. Two such simulants were employed in this research, Lunar Mare Simulant-1 (LMS-1), and Lunar Highlands Simulant-1 (LHS-1), which were added to cultures of human lung epithelial cells (A549) to simulate lung exposure to the dusts. In addition to pulverization, previously shown to increase dust toxicity sharply, the simulants were exposed to hydrogen gas at high temperature as a proxy for solar wind exposure. This treatment further increased the toxicity of both simulants, as measured by the disruption of mitochondrial function, and damage to DNA both in mitochondria and in the nucleus. By testing the effects of supplementing the cells with an antioxidant (N-acetylcysteine), we showed that a substantial component of this toxicity arises from free radicals. It remains to be determined to what extent the radicals arise from the dust itself, as opposed to their active generation by inflammatory processes in the treated cells.

Plain Language Summary With the Artemis program, humans will soon return to explore the Moon. However, lunar surface dust has toxic potential that must be assessed in order to clarify short-term and long-term health risks for Artemis astronauts. Numerous studies indicate that Moon dust has chemical and physical properties that may strongly affect dust toxicity. Unlike terrestrial dust, lunar regolith experiences "space weathering" under a vacuum, including the effects of solar wind, which further modifies the bulk and surface properties of this dust. In this work, we used two lunar dust simulant materials that were chemically treated to mimic the effects of space weathering. This treatment strongly increased all the toxic effects of both simulants: cell killing, mitochondrial dysfunction, and damage to DNA. Other experiments point to free radicals as a significant component of these effects. Future work will address whether these radicals arise from the simulants themselves or are generated by cellular activity.

1. Introduction

1.1. Dust Exposure and Pulmonary Disease

Occupational exposure to silica dust in mines underlies the development of diseases such as silicosis in humans (Hessel et al., 1988; Hnizdo et al., 1997; Hnizdo & Vallyathan, 2003; Merget et al., 2002). Other types of fine particles also exert toxicity and cause chronic pulmonary disease (Hsu et al., 2018; Hu et al., 2016; Medina-Reyes et al., 2015; Skuland et al., 2020). The properties of lunar dust suggest it to be a potential risk for humans if they are exposed (Linnarsson et al., 2012).

1.2. Lunar Dust

As shown in previous studies (Cain, 2010; Loftus et al., 2008; Wagner, 2006), Moon dust is highly reactive because of space weathering, including exposure to intense ultraviolet (UV) light, ionizing radiation, solar wind,

Project Administration: B. Demple
Resources: J. A. Hurowitz, H. Nekvasil
Software: J. Bauer
Supervision: J. A. Hurowitz, H. Nekvasil, B. Demple
Validation: J. H. M. Chang, Z. Xue, B. Wehle, D. A. Hendrix, T. Catalano
Writing – original draft: J. H. M. Chang, B. Demple
Writing – review & editing: J. H. M. Chang, Z. Xue, J. Bauer, B. Wehle, D. A. Hendrix, T. Catalano, J. A. Hurowitz, H. Nekvasil, B. Demple

and micrometeorite bombardment. The dust particles become finer, more jagged, and more reactive as a result of this weathering; indeed, lunar dust adhered strongly to spacesuits, thus bringing the material into the living areas and causing respiratory and other irritations (Colwell et al., 2007; Linnarsson et al., 2012; Pohlen et al., 2022).

1.3. Our Study

To build on our previous work (Caston et al., 2018; Hendrix et al., 2019), here we have applied new experimental techniques to assess the toxic effects of lunar dust simulants on cells. New lunar dust simulants were used as better mimics of the composition and properties of lunar regolith. We modeled solar wind effects artificially by exposing the simulants to strongly reducing conditions. The possible contribution of reactive oxygen species (ROS) to the toxic effects of lunar dust simulants (Hendrix et al., 2019; Linnarsson et al., 2012; Pohlen et al., 2022) was addressed by testing whether antioxidant supplementation of the cells affected the various toxic endpoints.

2. Materials and Methods

2.1. Cell Culture

Human lung alveolar epithelial (A549) cells were cultured at 37°C in Ham's F12-K (Kaighn's) nutrient medium (Gibco #21127022) supplemented with 10% fetal bovine serum (Corning #MT35010CV) and an antibiotic/antimycotic mix diluted 100-fold from the commercial stock solution (Sigma-Aldrich #A5955100-ML) (Caston et al., 2018). Cells were seeded in 6-well plates (Corning #3516) with supplemented medium at least 12 hr before the start of an experiment, except for those using the RESIPHER device (see Section 2.6). Dust or drug exposure was conducted in serum-free medium to avoid possible reactions with serum components such as antioxidants. For the cell survival and MitoSOX Red fluorescence assays, one well in each set contained only the supplemented medium (no cells) to serve as blank for fluorescence background; the other 5 wells were each seeded with 8×10^5 cells including a positive control treated with 20 μM Antimycin A (AA). The remaining wells were treated with 0.5, 1, or 1.5 mg/cm^2 of dust. For the comet assay, 6 wells were seeded with cells as above, 1 with cells only as a negative control, 4 treated with 1 mg/cm^2 of dust, and the sixth treated with 350 μM etoposide (a DNA topoisomerase inhibitor) as a positive control. The toxic challenges were performed for 1 hr, after which the medium was removed, and replaced with serum-containing medium (survival), Hank's balanced salt solution (HBSS) (MitoSOX), or phosphate-buffered saline (PBS) (Corning #46-013-CM) (PBS is 137 mM NaCl, 2.7 mM KCl, 10 mM Na$_2$HPO$_4$, 1.8 mM KH$_2$PO$_4$). For the polymerase chain reaction (PCR) assays, the positive control was 1 mM H$_2$O$_2$, and dust treatment was 0.5 mg/cm^2 or 1.5 mg/cm^2 for 1 hr, and the medium was removed and replaced with PBS, after which the DNA was extracted. For pretreatment with N-acetylcysteine (NAC), pilot experiments explored concentrations of 0.05–5 mM NAC for 2–24 hr based on published studies (Mitsopoulos & Suntres, 2011) for protection of A549 cells against H$_2$O$_2$ toxicity. Based on those results, a standard protocol was established: cells were incubated in normal growth medium, and half of the wells were supplemented with freshly prepared 5 mM NAC for 24 hr before a toxic challenge, with NAC supplementation continued in the post-challenge incubation.

2.2. General Preparation of Simulant Materials

The Lunar Mare Simulant-1 (LMS-1) and the Lunar Highlands Simulant-1 (LHS-1) used in this study were purchased from EXOLITH Lab (532 S Econ Cir, Oviedo, FL 32765, USA). Both are composed of terrestrial minerals and glass, and have higher Na and K, and lower Fe, Mg, and Ca contents than typical lunar regolith (Long-Fox et al., 2023). To produce the finest regolith size fraction for the study (<10 μm), the simulants were sieved through 63-μm mesh, and crushed in a Retsch PM 100 planetary agate ball mill down to an average grain size <10 μm and including <1 μm particles (see Table C.2 in Hendrix (2022)). The distribution of particle sizes was determined using a Malvern Instruments Mastersizer 2000. Surface areas of samples were measured by gas adsorption using ultra-high purity nitrogen gas via six-point Brunauer-Emmett-Teller theory on a NOVA-2000 BET analyzer as described (Hendrix et al., 2021). The resulting material was a fine powder composed of angular, mechanically crushed grains.

2.3. Artificial Space Weathering of Simulant Materials

Pulverization of simulant materials (to mimic some effects of impact gardening) substantially increases their toxicity (Caston et al., 2018) and was performed in every case in the current work. To mimic the effect of solar
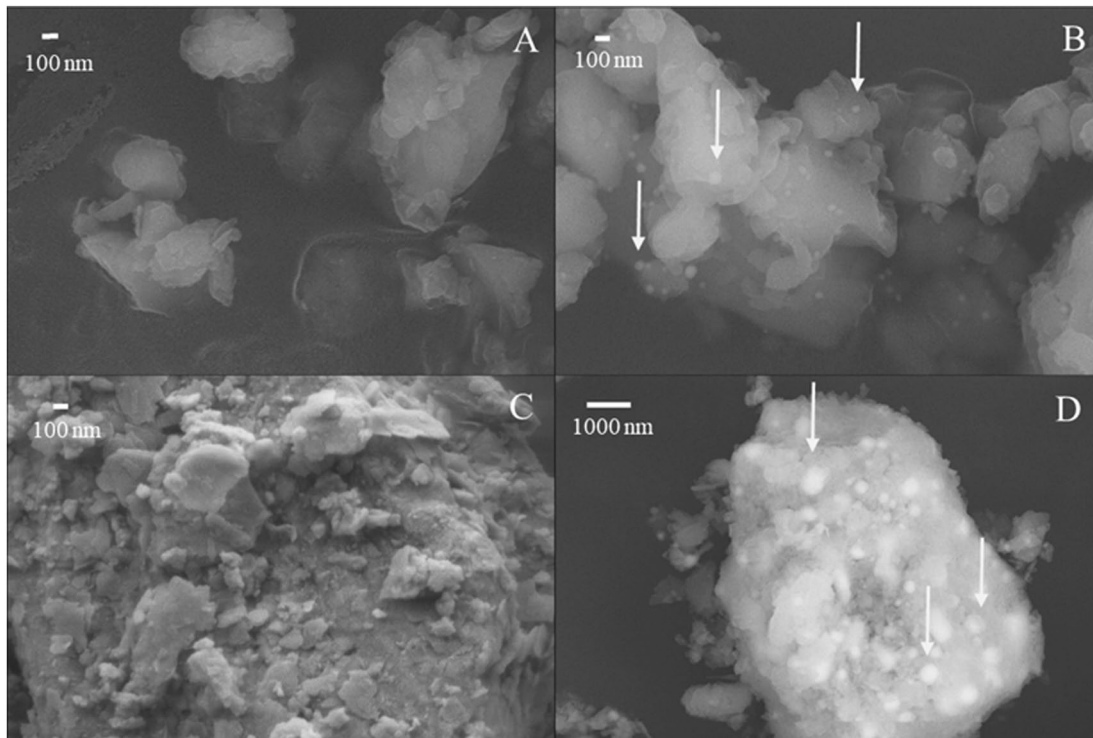
Figure 1. Close-up scanning electron microscopy images of lunar simulants before and after reduction treatment. Note the different image scales. (a) LHS-1, (b) LHS-1 after reduction, (c) LMS-1, (d) LMS-1 after reduction. Reduced simulants show the development of Fe nanoparticles on grain surfaces. Arrows point to some Fe nanoparticles.

wind and micrometeorite bombardment on the dust properties, ground simulants were reduced in hydrogen gas similar to the process described in Allen et al. (1994). Sample powder for reduction was poured into a silica glass boat and evenly distributed across the bottom in about a 1 mm thick layer. This boat was then loaded into a horizontal silica glass tube sealed at both ends by rubber stoppers with hose connections for gas flow. The tube was placed in an externally heated tube furnace with a type K thermocouple placed at the hotspot to monitor temperature. Before the furnace was turned on, the tube was purged with H_2 for 10 min. After purging, the furnace was brought up to 900°C and held for 10 min. After the heat treatment, the silica glass tube, with H_2 flowing through, was removed from the furnace and cooled with water-soaked towels. The gas was turned off, the sample removed, and the sample was immediately put into a vacuum desiccator.

This treatment resulted in partial sintering of the material, and the formation of metallic iron nanoparticles (Figure 1). After processing, the samples were stored in a vacuum of approximately 25 mmHg (ca. 0.03 atm) and room temperature. Just before cell treatment experiments, the relevant materials were weighed out and transported under vacuum to the cell treatment laboratory. Immediately before use with cells, individual samples were re-ground for 3 min with an agate mortar and pestle (freshly cleaned with 70% ethanol and dried before use) by hand. The samples were used within 25 min of re-grinding.

2.4. Cell Treatment and Survival Assay

The freshly re-ground samples were added directly to cells in serum-free culture medium, with gentle rotation to ensure distribution of the grains. Vigorous mixing was not possible without disrupting cellular contact with the plate. The sample addition was followed by a 1-hr incubation at 37°C. The cells were then rinsed with sterile PBS to wash most dust particles away. Following dust exposure, the washed cells were incubated another 24 hr in serum-containing growth medium. After removal of the medium, the cells were recovered by the addition 0.5 mL of a solution containing 0.25% trypsin and 2.21 mM EDTA (Corning# 25-053-Cl). After 3 min at 37°C, 0.5 mL of serum-supplemented medium was added to neutralize the trypsin. After gently mixing, 10-µL aliquots of cell solution were mixed with 10-µL aliquots of 0.4% trypan blue dye (Sigma #T8154). The stained cell samples were

counted on a hemocytometer under a microscope, with the blue-stained cells scored as dead (Strober, 2001). The control count was normalized to 100% viability (Caston et al., 2018).

2.5. MitoSOX Red

The protocol was based on a previous study (Wojtala et al., 2014). A 5 mM stock solution of MitoSOX Red Mitochondrial Superoxide Indicator (Invitrogen #M36008) was prepared in dimethyl sulfoxide and stored at −20°C. Immediately before use with the cell samples, the MitoSOX Red stock was diluted to 0.5 µM with HBSS: 140 mM NaCl, 5 mM KCl, 1 mM $CaCl_2$, 0.4 mM $MgSO_4 \cdot 7H_2O$, 0.5 mM $MgCl_2 \cdot 6H_2O$, 0.3 mM Na_2HPO_4, 0.4 mM KH_2PO_4, 6 mM glucose, 4 mM $NaHCO_3$ (Hanks, 1975). Freshly reground lunar regolith simulants were added directly to each well. After the exposure, the cells were washed twice with 2 mL of HBSS, followed by the addition of 0.5 µM MitoSOX Red solution in HBSS, and the incubation continued for 1.5 hr at 37°C. The cells were then washed twice with 2 mL HBSS. Fluorescent microscope images were acquired using a BioTek Lionheart Imager, with excitation at 580 nm and emission at 650 nm. The cells were then released by trypsinization for 3 min, which was stopped by adding serum-containing medium. The cells were then collected by centrifugation at $600 \times g$ for 5 min, and resuspended with HBSS buffer at 8×10^4 cells per mL. To measure total fluorescence, a 100 µL-aliquot of the cell suspension was placed in each well of a 96-well plate (Thermo Scientific #265301). Quantification of the fluorescence was done using a Molecular Devices SpectraMax M5 Microplate Reader, with excitation at 510 nm, and emission measured at 580 nm. The background fluorescence was subtracted, and the controls were normalized to 1.

2.6. Real-Time Detection of Oxygen Consumption Rate

The RESIPHER device (Lucid Scientific, Atlanta, GA) allows the real-time detection of oxygen consumption by cells, with multiple samples measured simultaneously in 96-well plates (Thermo Scientific #167852) and for extended times. For these experiments, aliquots of 2×10^5 cells per well were seeded 24 hr prior to treatment and incubated at 37°C; all samples were set up in four replicates. The O_2-sensing lids were added after the cells are settled in each well. Non-reduced or reduced LMS-1, suspended in 200 µL of serum-free cell culture medium, was applied at 0.05, 0.1, 0.2, or 0.5 mg/cm² into individual wells. As a positive control for mitochondrial disruption, the Complex III inhibitor AA was added at 20 µM. During the exposure to AA or the dust particles, the O_2-sensing lid was temporarily replaced with a normal lid. After a 1 hr-challenge with LMS-1, the serum-free medium in each well was removed and replaced with supplemented medium, and the O_2-sensing lid was added to the plate again. The oxygen sensors continuously monitor the oxygen concentration in the culture media, with measurements taken automatically every 36 s for every well. As the cells consume oxygen, an oxygen concentration gradient is generated, with the rate of O_2 consumption calculated by the software continuously up to 72 hr in our experiments. With the high sensitivity of this instrument, at least 2 hr were usually required for the incubation chamber to re-equilibrate. The data were analyzed based on instructions from the manufacturers using GraphPad Prism.

2.7. Quantitative Polymerase Chain Reaction (PCR) Assay

For this analysis, immediately after a 1 hr-challenge with dust or other agents, total cellular DNA was extracted using the QIAGEN 20/G DNA extraction kit (Qiagen #10223). DNA concentrations were quantified using a NanoDrop ND-1000 Spectrophotometer. The PCR assay protocols here were slightly revised from previous protocols (Ayala-Torres et al., 2000; Caston et al., 2018; Furda et al., 2014). For "long" mitochondrial PCR (amplifying about half of the mitochondrial DNA molecule, 15 ng of DNA template was mixed with LongAmp buffer and 100 U/mL of LongAmp Taq polymerase [New England Biolabs #M0323S], 300 µM each of the four deoxynucleoside triphosphates, and 400 nM each of the forward and reverse primers [see Table 1], in a total volume of 50 µL). The thermocycler was set for 3 min at 95°C for the initial denaturation, followed by 20 cycles of 15 s at 95°C for denaturation and 9 min at 60°C for primer annealing and extension, and a 21st cycle with a final extension at 65°C for 10 min. For the "short" mitochondrial PCR, 25 ng of DNA template was mixed with ThermoPol buffer and 25 U/mL of ThermoPol Taq polymerase (New England Biolabs #M0267S), 150 µM each of the four deoxynucleoside triphosphates, and 1 µM each of the forward and reverse primers (Table 1), in a total volume of 50 µL. The thermocycler program for short PCR was 2 min at 95°C for the initial denaturation,

Table 1
Forward and Reverse Primers Used in the Quantitative Polymerase Chain Reaction Assay

Primers used	Sequence (5′→3′)
Human mitochondrial long, sense strand	TCTAAGCCTCCTTATTCGAGCCGA
Human mitochondrial long, antisense strand	TTTCATCATGCGGAGATGTTGGATGG
Human mitochondrial short, sense strand	CCCCACAAACCCCATTACTAAACCCA
Human mitochondrial short, antisense strand	TTTCATCATGCGGAGATGTTGGATGG

followed by 22 cycles of 15 s at 95°C for denaturation, 30 s at 56°C for annealing, 1 min at 68°C for extension, and finished with a final extension at 68°C for 5 min. The long PCR product is 8,843 base pairs, and the short PCR product is 222 base pairs. The PCR products were quantified using the Picogreen reagent (Thermo-Fisher P11496) to detect double-stranded DNA, with the fluorescent signals acquired from a Molecular Devices SpectraMax M5 Microplate Reader. Since the long PCR reaction has a much greater chance of encountering a lesion in the template than is the case for the short PCR reaction, the ratio of their products reflects the DNA damage level. The controls were normalized to a ratio of 1.

2.8. Alkaline Comet Assay

The alkaline comet assay was used to detect both single-strand breaks and double-strand breaks in DNA in the cell nucleus. Our protocol was adapted from published studies (Muruzabal et al., 2021; Nowsheen et al., 2012; Tice et al., 2000). Following dust treatment and trypsinization, the recovered cell number was estimated using a hemocytometer. Next, 20 μL of cell suspension containing ∼6,000 cells was mixed with 180 μL 1% low-melting-point agarose gel (SeaPlaque GTG Agarose #50110) at 37°C. The agarose-cell suspension was then placed on warmed glass microscope slides (180 μL per slide), which were cooled to room temperature to allow the gel to set. Lysis buffer with the concentration of 2.5 M NaCl, 0.1 M $Na_2EDTA \cdot H_2O$, and 0.01 M Tris was first prepared and then adjusted to pH = 10 with NaOH with final concentration of 0.03 M L-lauroyl sarcosine sodium salt stirred in the lysis buffer. After the gels had set, they were incubated in the mixture of 66.75 mL lysis buffer, 7.5 mL DMSO, and 0.75 mL of Triton X-100 at 4°C for 1 hr. The slides were then transferred to a neutralizing buffer containing 4 M Tris (adjusted to pH = 7.5 with NaOH before use) to remove the lysis buffer, then incubated with the alkaline electrophoresis buffer containing 0.3 M NaOH and 1 mM $Na_2EDTA \cdot H_2O$. The slides were subjected to electrophoresis at 20 V/cm for 20 min. Following electrophoresis, the slides were dried overnight at room temperature, then stained with 0.5 mL SYBR Gold (Invitrogen #S11494) for microscopic visualization. Images of the stained cells were obtained using a Nikon E400. Images were processed using ImageJ to remove the auto-fluorescent signals of the dust particles. At least 100 cells were analyzed for each sample through OpenComet as described (Gyori et al., 2014).

2.9. Statistical Analyses

At least three biological replicates were used for each control and experimental group. Student's *T*-test with Tukey's method were used for comparisons between the controls and the various treatment groups. Results were considered significant when the *p*-value for comparison was ≤0.05 (see individual figure legends). The error bars show standard deviations.

3. Results

3.1. Cell Viability After Exposure to LMS-1 and LHS-1

We tested the possible contribution of solar wind-mediated space weathering to simulant toxicity by comparing the cytotoxicity of untreated and artificially reduced simulants. Cell survival was scored with the trypan blue exclusion assay (see Materials and Methods). Non-reduced LMS-1 (Figure 2a) and LHS-1 (Figure 2b) were both clearly cytotoxic even at the lowest exposure (0.5 mg/cm^2). Importantly, the cytotoxicity of both materials was strongly enhanced by the reducing treatment (Figures 2a and 2b).

To test the possible role of free radicals and oxidative damage in the cytotoxicity of the simulants, we supplemented the cells with NAC, which both is an antioxidant itself and boosts the capacity of cellular reducing pathways (Ates et al., 2008). Pilot experiments determined the effective level of the antioxidant, with the best protection achieved using 5 mM NAC supplementation 24 hr before dust exposure, and the continued presence of
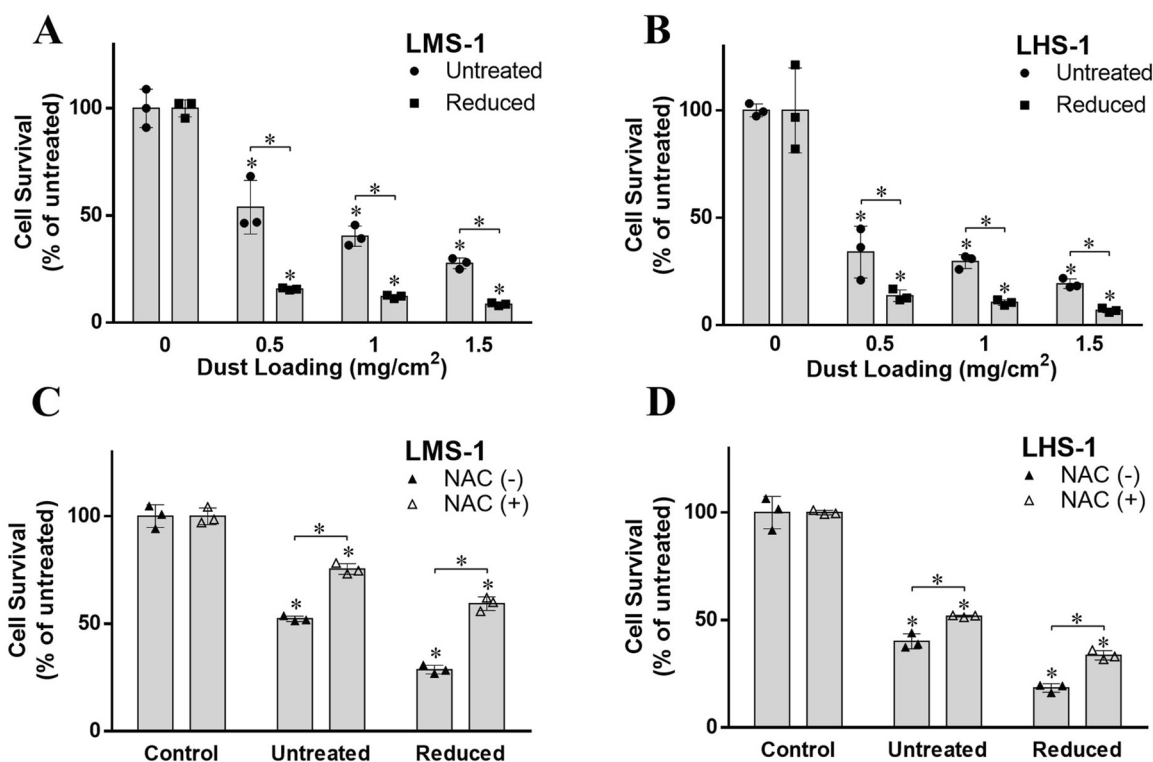
Figure 2. Viability of human lung alveolar epithelial cells exposed to LMS-1 or LHS-1 and effects of artificial space weathering and antioxidant supplementation. A549 cells were exposed for 1 hr with the indicated amounts of freshly-ground simulants (a) LMS-1 or (b) LHS-1, using the reduced forms where indicated. The dust was then removed, and the growth medium replaced. After incubation for a further 24 hr, cell viability was scored by trypan blue exclusion. Where indicated, N-acetylcysteine (NAC) was added 24 hr before the 1-hr exposure to (c) LMS-1 or (d) LHS-1, each at 0.5 mg/cm^2, and the NAC supplementation was continued after the dust treatment. * denotes p-values <0.01 compared to controls or comparisons in specified groups. The error bars are standard deviations ($n = 3$).

the antioxidant after the exposure. NAC supplementation increased cell survival both for LMS-1 (Figure 2c) and for LHS-1 (Figure 2d) exposures of 0.5 mg/cm^2.

Given the likely role of the particle surface in toxicity (Pohlen et al., 2022), we computed the initial rates of cell-killing as a function of the particle surface area. That computation (Table 2) also confirmed (a) that LHS-1 was more toxic than LMS-1 ($p < 0.01$ for all comparisons between LMS-1 and LHS-1), (b) that the reducing treatment significantly enhanced the toxicity of both types of simulants ($p < 0.01$ for all comparisons between non-reduced and reduced materials), and (c) that the antioxidant supplementation increased cell survival in all cases ($p < 0.01$ for all comparisons between NAC-pretreated cells vs. non-supplemented controls).

3.2. Mitochondrial DNA Damage After Exposure to LMS-1 and LHS-1

Our previous study (Caston et al., 2018) showed dust-dependent damage to mitochondrial DNA by other lunar dust simulants. For the new materials, we used the same assay based on PCR, in which DNA damage is reported

Table 2
Cell-Killing Rates Normalized to Dust Surface Area

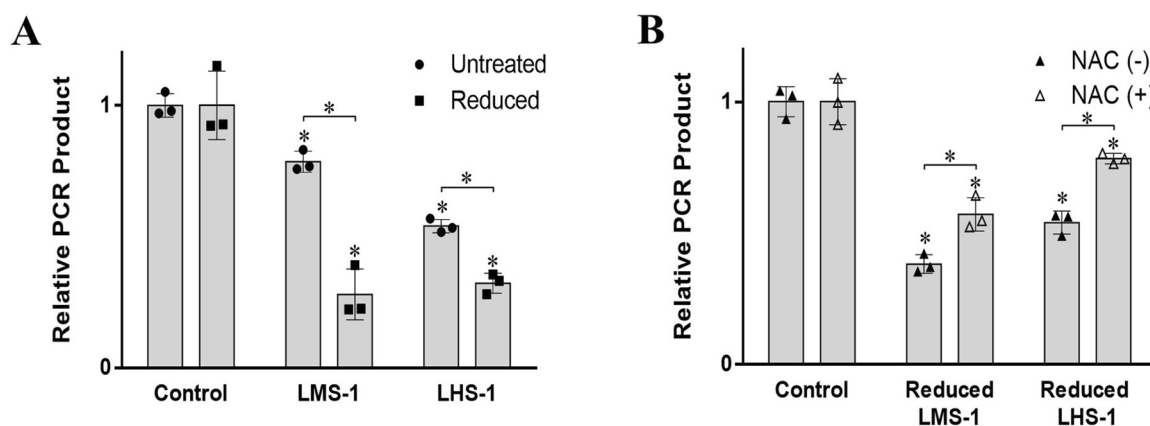| Lunar dust simulant	Cell-killing by 0.5 mg/cm^2 dust (% per hr)		Total dust surface area (cm^2)	Cell killing rate (% per hr per cm^2 of surface)	
	No NAC	NAC supplemented		No NAC	NAC supplemented
LMS-1	48	25	430	0.11	0.06
Reduced LMS-1	71	41	200	0.36	0.21
LHS-1	60	48	280	0.21	0.17
Reduced LHS-1	82	66	160	0.51	0.41

Figure 3. Simulant-induced mitochondrial DNA damage. (a) Freshly-ground LMS-1 or LHS-1, with or without prior reducing treatment, were added at 1.5 mg/cm^2 to cells in 6-well plates, and after 1 hr, total DNA was immediately extracted for the Polymerase Chain Reaction (PCR) assay. (b) Protection by antioxidant supplementation. Reduced and freshly-ground reduced LMS-1 or LHS-1 were added after N-acetylcysteine (NAC) pretreatment where indicated, and after 1 hr, total DNA was immediately extracted for the PCR assay. * denotes *p*-values <0.01 compared to controls or comparisons in specified groups. The error bars are standard deviations ($n = 3$).

as a diminished product signal (Ayala-Torres et al., 2000; Furda et al., 2014). The integrity of mitochondrial DNA was decreased immediately after a 1 hr-exposure to non-reduced LMS-1 or non-reduced LHS-1, with the latter generating more damage (Figure 3a). The reducing treatment increased the mtDNA damaging property of both simulants, but the genotoxicity of the two reduced materials was not significantly different (Figure 3a). As seen for the cell survival results, mitochondrial DNA damage by both of the reduced simulants was strongly diminished by the antioxidant supplementation of the cells (Figure 3b). In summary, the reduced materials caused greater damage to mitochondrial DNA than did the unreduced simulants, and NAC supplementation gave a consistent protective effect.

3.3. Mitochondrial Function After Exposure to LMS-1 and LHS-1

The observed rapid damage to mitochondrial DNA poses the question of whether mitochondrial function was affected. To address this issue, we used the cationic dye MitoSOX Red, which enters mitochondria and forms a fluorescent signal after reaction with superoxide, the initial product of disrupted respiratory chains in these organelles (Kowaltowski et al., 2009). As seen for the other measures, both LMS-1 and LHS-1 caused significant mitochondrial disruption within the 1 hr-exposure (Figures 4a and 4b). Mitotoxicity was enhanced for the reduced compared to non-reduced materials. And once again, the mitotoxicity was in all cases significantly diminished by antioxidant supplementation. Some examples of increased MitoSOX Red staining in untreated dust-exposed cells are shown in Figure 4c. These results show that exposure to lunar dust simulants can rapidly damage mitochondrial DNA and disrupt mitochondrial function in A549 cells.

3.4. Real-Time Oxygen Consumption in Cells After Exposure to LMS-1

Mitochondria generate energy in the form of adenosine triphosphate, largely dependent on the consumption of oxygen (Kowaltowski et al., 2009). Given the rapid disruption of mitochondrial function in dust-exposed cells, we tested a more direct technique for monitoring the activity of the organelle. This approach monitored O$_2$ consumption continuously in multiple samples over several days (see Materials and Methods). Pilot experiments established that we could detect mitotoxicity caused by amounts of dust 10-fold lower than needed for the other assays. Fluctuations of O$_2$ consumption during the first ~6 hr are due to the time needed for oxygen equilibration of the incubation chamber and the culture medium in the plate wells. Untreated cells continued to consume O$_2$ at a rate that increased over the first 48 hr as cell proliferation continued, leveling off as the cells multiplied to fill the test well area. Even the lowest level of *non-reduced* LMS-1 dampened O$_2$ metabolism and partly suppressed the increase over 72 hr (Figure 5a). Higher levels of non-reduced LMS-1 further suppressed O$_2$ consumption in a somewhat dose-dependent manner (Figure 5a). Even the lowest level of reduced LMS-1 was about as mitotoxic as the highest level of non-reduced material, with a clear dose effect at higher levels of treatment (Figure 5b). The highest level of reduced LMS-1 suppressed respiration nearly as profoundly did the positive control AA, which blocks the respiratory chain immediately before the
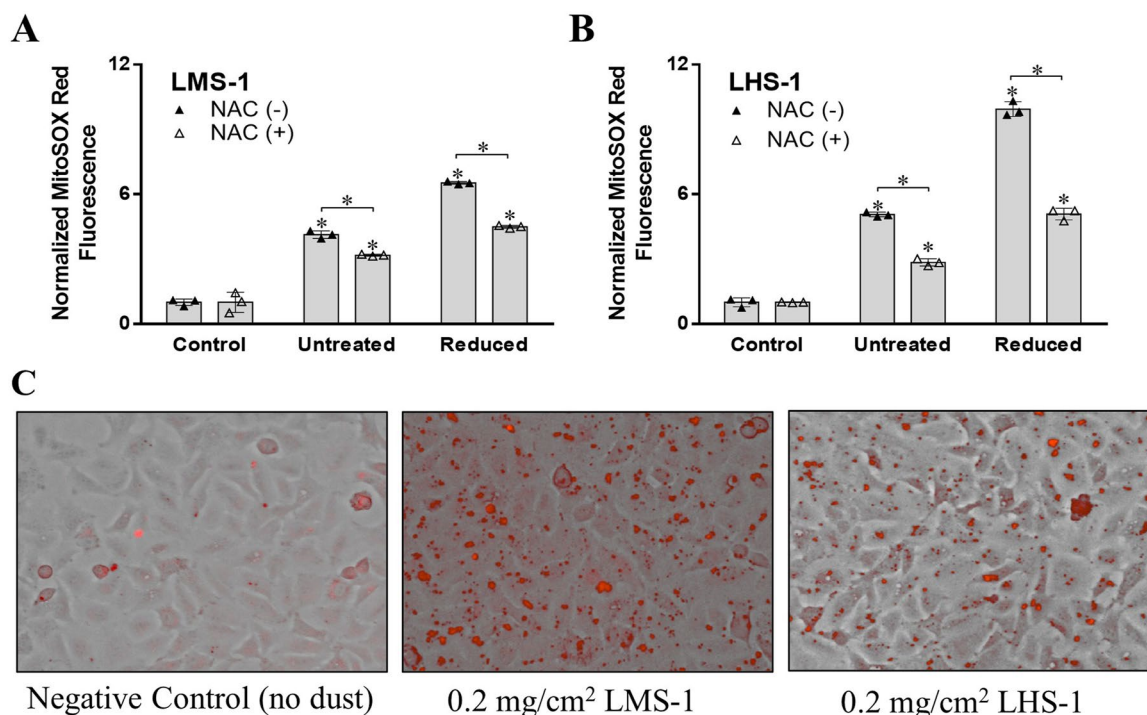
Figure 4. MitoSOX Red fluorescence after exposure to simulants. Freshly-ground LMS-1 (a) or LHS-1 (b) were added at 0.5 mg/cm² to A549 cells for 1 hr and the dust removed, followed by a 1.5-hr incubation with the MitoSOX Red redox-sensitive dye. (a, b) Quantified MitoSOX Red fluorescent signals. (c) Examples of MitoSOX Red staining. * denotes p-values <0.01 for the indicated comparisons. The error bars are standard deviations ($n = 3$).

O_2-consuming step (Figure 5b). The reduced materials combined with cells all produced an early and transient peak of O_2 consumption. It is unclear whether the transient O_2 consumption is biological, but in experiments with dust alone, we have not detected any measurable oxygen consumption. It is clear, however, that this approach allows dust toxicity to be revealed with greater sensitivity and over a more extended period after exposure.

3.5. Nuclear DNA Damage From Exposure to Lunar Dust Simulants

In a prior study (Caston et al., 2018), we showed using a PCR-based assay that exposure to other lunar regolith simulants caused damage to DNA in the nucleus. However, the PCR assay for nuclear DNA, with just two copies per cell of the target segment for the assay, is rather noisy compared to that for mitochondrial DNA (with hundreds of copies per cell). We therefore used the "comet assay," which detects DNA breaks by the mobilization
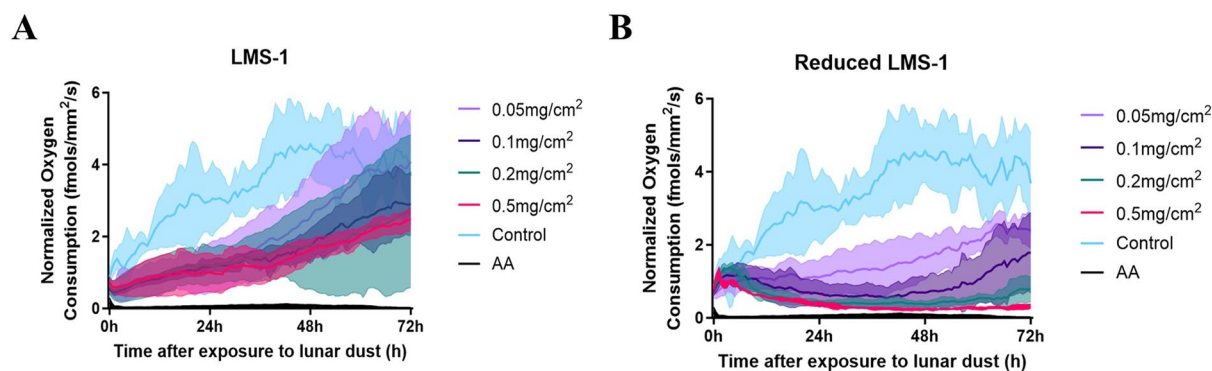

Figure 5. Normalized oxygen consumption rate in simulant-exposed cells. The RESIPHER instrument (LUCID Scientific) continuously measures real-time O_2 consumption by cells in culture. A549 cells were exposed to (a) non-reduced or (b) reduced LMS-1 (each $n = 2$–4) at 0.05, 0.1, 0.2, or 0.5 mg/cm², and O_2 consumption was monitored continuously over the next 72 hr. Antimycin A (AA) is a mitochondrial inhibitor, used as a positive control for mitochondrial dysfunction. The 95% confidence intervals are shown for each curve.
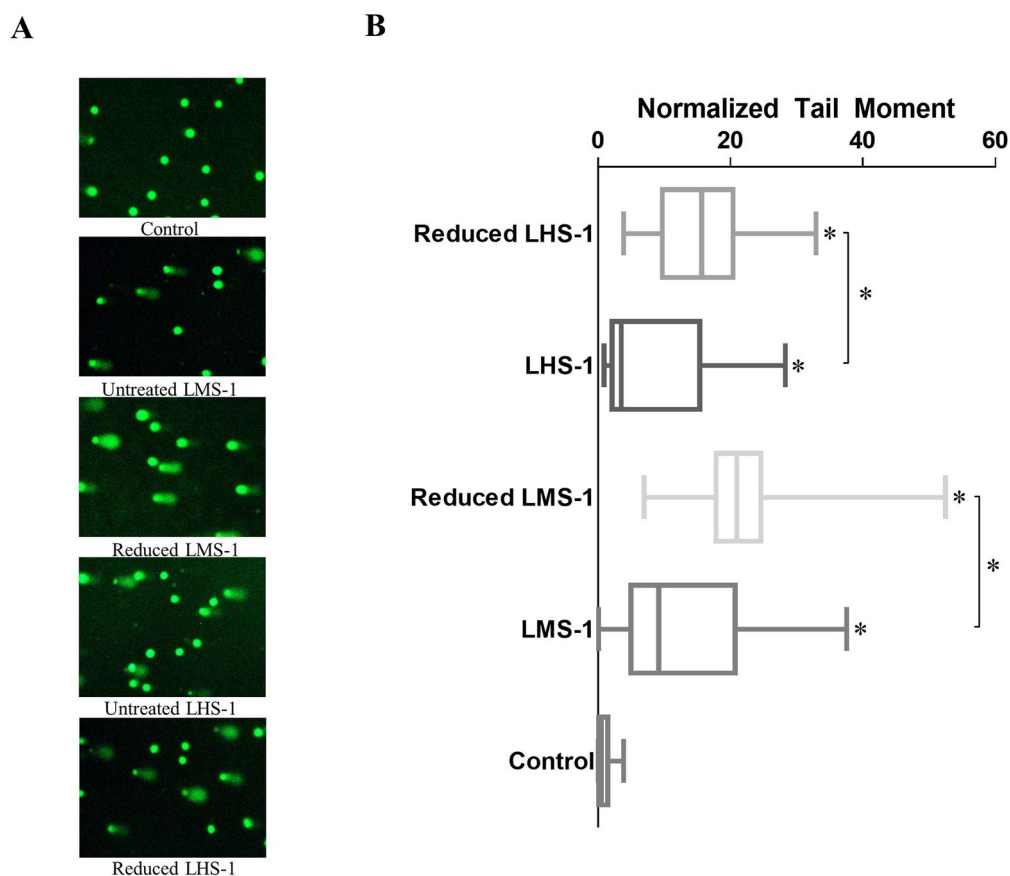
A **B**

Figure 6. Alkaline comet assay for DNA damage. Freshly-ground LMS-1 or LHS-1 were added at 1 mg/cm² to A549 cells for a 1 hr-exposure, and the samples were processed as described in Materials and Methods. (a) Examples of the fluorescent images. Electrophoresis was from left (-pole) to right (+pole). (b) The extent of DNA damage was computed from the length and intensity of the comet-like tails (called the tail moment), with the control value normalized to 1. * Denotes p-values <0.01 for the indicated comparisons. The error bars are standard deviation ($n = 100$).

of the DNA from the nucleus during electrophoresis (examples in Figure 6a; see Materials and Methods). That approach revealed DNA damage caused by both simulants, which appeared to be enhanced by the reducing treatment of the materials (Figure 6b). We note the large variability in these experiments, which may reflect the point in the cell cycle at which the exposure and analysis occurred. For example, cells in S-phase or mitosis are expected to be more sensitive to genotoxic treatments of all kinds. It is clear that, as seen for mitochondrial DNA damage (Figure 3), nuclear DNA is harmed as an early effect of dust exposure.

4. Discussion

4.1. Summary of Findings

Our new findings can be summarized as follows: (a) artificial space weathering to simulate combined micrometeorite bombardment and solar wind exposure enhanced all aspects of toxicity for both simulant materials; (b) free radicals/ROS are significant components of all aspects of toxicity for both simulants; (c) direct monitoring of cellular O_2 consumption revealed the toxic impact of the simulants at levels 10-fold lower than did the other assays, which was enhanced by the reducing treatment; there was partial recovery from the lowest level of non-reduced LMS-1, and little to none from higher non-reduced dust levels or from any level of reduced LMS-1, indicating irreversible mitochondrial damage.

4.2. Enhanced Toxicity of Lunar Dust Simulants With Artificial Space Weathering

The consistent and strong increase in toxicity by simulating the space weathering effects of solar wind and micrometeorite bombardment indicates that it is likely to be an important aspect of lunar regolith toxicity. Certainly,

Table 3
Composition of LHS-1 and LMS-1 (Weight Percent)

Phase	LHS-1 (%)	LMS-1 (%)
Plagioclase	74.4	19.8
Glass	24.2	24.5
Pyroxene	0.3	32.8
Basalt	0.5	7.5
Ilmenite	0.4	4.3
Olivine	0.2	11.1

this observation underscores the need to investigate freshly-collected samples of lunar regolith to test this hypothesis with actual lunar materials. Electron microscopy showed that the reducing treatment produces surface deposits of iron on the particles (Figure 1). However, the somewhat greater toxicity of LHS-1 in some assays, despite its lower abundance of Fe-bearing minerals (Table 3) and lower bulk FeO content (Table 4) makes it difficult to assess what is causing the enhanced toxicity of LHS-1. Other heavy metals present on the Moon may also deposit on the lunar dust particles (Allen et al., 1994), which potentially leads to a more intricate mechanisms of toxicity due to the interaction of the lunar dust simulant particles and the cells. Additional studies should address this issue more closely, including tests of other likely space-weathering effects, such as ionizing radiation or UV light. Obviously, it would be very interesting to test actual lunar regolith samples, especially more recently collected materials as they are recovered. In any case, it is unlikely that the toxic effects of the simulants (or lunar dust itself) are due to any single component.

4.3. ROS: A Key Component of the Toxicity of Lunar Dust Simulants

While the reducing treatment enhances the ability of simulants to produce ·OH radicals in an aqueous environment (Hendrix, 2022), the role of this oxidative activity in cellular damage is uncertain. The broad protective effects of antioxidant supplementation support the view that ROS is an important component of simulant toxicity. However, the amount of direct radical production by the dust appears to be modest (Hendrix et al., 2019). In another study, ·OH production by various simulant dusts did not correlate with toxicity in the lungs of rats (Lam et al., 2022).

4.4. Potential Impact of Long-Term Exposure to Lunar Dust in Human Cells

While the reducing treatment enhances the ability of simulants to produce ·OH radicals in an aqueous environment (Hendrix, 2022), the role of this oxidative activity in cellular damage is uncertain. We previously found no direct correlation between ·OH production and cytotoxicity (Caston et al., 2018). Mammalian cells themselves actively produce toxic levels of ROS when suitably stimulated, for example, by exposure to silica dust (Skuland et al., 2020), titanium oxide (Skocaj et al., 2011), or other fine metallic dust (Cambre et al., 2020), which can continue after the initial exposure (Kuznetsov et al., 2017; Linnarsson et al., 2012; Pohlen et al., 2022). Particles that enter deeply into the lungs and lodge in the alveoli can cause persistent local inflammation, which is associated with a strong cancer risk (Merget et al., 2002; Ovrevik et al., 2002; Saraf et al., 1999; Skuland et al., 2020; Xu et al., 2020). If lunar dust similarly causes persistent local ROS generation in the lungs, which seems likely in view of what we know, that would constitute a significant long-term health risk for lunar explorers. Damage leading to long-term health consequences is also possible for other tissues (e.g., the eyes) (Braddock, 2021; Heiken et al., 1991; James & Kahn-Mayberry, 2009; Lam et al., 2022).

Damage to mitochondria, which are vital organelles in the cell, and disruption of mitochondrial energy production, was documented in multiple ways in this study. In addition to acting as a source of persistent inflammatory ROS, mitochondria can trigger other cell signaling pathways, including those that activate cell death mechanisms (Mittal et al., 2014; Ryter et al., 2007; Van Houten et al., 2016). Consequently, tissue damage would be a significant short-term risk for lunar regolith exposure, via tissue loss or derangement in the exposed organs. Engineering controls should be able to mitigate much of the short-term risk by minimizing explorer exposure to Moon dust. However, incidental or accidental exposure is hard to prevent completely (Braddock, 2021; Cain, 2010; Winterhalter et al., 2020). Assays at low exposure levels would be helpful in this regard in establishing levels where there is no detectable impact. We have made a step in that direction by showing that

Table 4
Oxide Content of Lunar Dust Simulants (Weight Percent)

Oxide	LHS-1	LMS-1
SiO_2	44.18	42.81
TiO_2	0.79	4.62
Al_2O_3	26.24	14.13
Cr_2O_3	0.02	0.21
FeO	3.04	7.87
MnO	0.05	0.15
MgO	11.22	18.89
CaO	11.62	5.94
Na_2O	2.30	4.92
K_2O	0.46	0.57
P_2O_5	0.00	0.44
SO_3	0.10	0.11
Total	100.00	100.00

the RESIPHER device enables us to detect substantial disruption of mitochondria at lower dust exposure levels than seen with the other assays.

4.5. Prospective Health Hazard Monitoring Technologies for Artemis Astronauts

The possible health hazards of lunar dust exposure might seem minor in comparison with other likely risks for Artemis explorers (Pohlen et al., 2022). However, the cell and tissue effects of exposure to such materials can have a long-term impact (Cain, 2010; James & Kahn-Mayberry, 2009; Kuznetsov et al., 2017; Linnarsson et al., 2012), which should be offset in favor of astronaut health. One way by which the research we present contributes is to point the way for the development of portable instruments to use for reporting dust toxicity during exploration of the Moon's surface. For example, improvements to lung-on-a-chip approaches (Skuland et al., 2020; Xu et al., 2020; Zhang et al., 2018) could provide increasingly useful bioassay devices that lunar explorers can use for their own protection by assessing the toxic potential of their immediate environment. In principle, such devices might be engineered to contain cells from individual explorers to allow a greater assessment of individual explorer risk.

Such real-time risk assessment could employ cell survival as an endpoint, but it would likely be more useful to measure early biomarkers of inflammation, such as the expression of cytokines generated by the exposed cells (Meindl et al., 2021; Skuland et al., 2020). In principle, disruption of respiration (mitochondrial function; see Figure 5) could also be a useful and sensitive measurement, as such disruption is a rapid effect of exposure to dust simulants, and it occurs at lower levels of dust exposure than cytotoxicity.

Conflict of Interest

The authors declare no conflicts of interest relevant to this study.

Data Availability Statement

Data are available at Chang et al. (2023).

References

Allen, C. C., Morris, R. V., & Mckay, D. S. (1994). Experimental reduction of lunar mare soil and volcanic glass. *Journal of Geophysical Research*, 99(E11), 23173–23185. https://doi.org/10.1029/94je02321

Ates, B., Abraham, L., & Ercal, N. (2008). Antioxidant and free radical scavenging properties of N-acetylcysteine amide (NACA) and comparison with N-acetylcysteine (NAC). *Free Radical Research*, 42(4), 372–377. https://doi.org/10.1080/10715760801998638

Ayala-Torres, S., Chen, Y., Svoboda, T., Rosenblatt, J., & Van Houten, B. (2000). Analysis of gene-specific DNA damage and repair using quantitative polymerase chain reaction. *Methods*, 22(2), 135–147. https://doi.org/10.1006/meth.2000.1054

Braddock, M. (2021). Hazards of lunar regolith for respiratory, central nervous system, cardiovascular and ocular function. In *The human factor in the settlement of the Moon: An interdisciplinary approach* (pp. 141–157).

Cain, J. R. (2010). Lunar dust: The hazard and astronaut exposure risks. *Earth, Moon, and Planets*, 107(1), 107–125. Journal article. https://doi.org/10.1007/s11038-010-9365-0

Cambre, M. H., Holl, N. J., Wang, B., Harper, L., Lee, H. J., Chusuei, C. C., et al. (2020). Cytotoxicity of NiO and Ni(OH)$_2$ nanoparticles is mediated by oxidative stress-induced cell death and suppression of cell proliferation. *International Journal of Molecular Sciences*, 21(7), 2355. https://doi.org/10.3390/ijms21072355

Caston, R., Luc, K., Hendrix, D., Hurowitz, J. A., & Demple, B. (2018). Assessing toxicity and nuclear and mitochondrial DNA damage caused by exposure of mammalian cells to lunar regolith simulants. *GeoHealth*, 2(4), 139–148. https://doi.org/10.1002/2017gh000125

Chang, J. H. M., Xue, Z., Bauer, J., Wehle, B., Hendrix, D., Catalano, T., et al. (2023). Artificial space weathering to mimic solar wind enhances the toxicity of lunar dust simulants in human lung cells [Dataset]. Dryad. https://doi.org/10.5061/dryad.mw6m9062w

Colwell, J. E., Batiste, S., Horanyi, M., Robertson, S., & Sture, S. (2007). Lunar surface: Dust dynamics and regolith mechanics. *Reviews of Geophysics*, 45(2), 45–70. https://doi.org/10.1029/2005rg000184

Furda, A., Santos, J. H., Meyer, J. N., & Van Houten, B. (2014). Quantitative PCR-based measurement of nuclear and mitochondrial DNA damage and repair in mammalian cells. *Methods in Molecular Biology*, 1105, 419–437. Retrieved from https://www.ncbi.nlm.nih.gov/pubmed/24623245

Gyori, B. M., Venkatachalam, G., Thiagarajan, P. S., Hsu, D., & Clement, M. V. (2014). OpenComet: An automated tool for comet assay image analysis. *Redox Biology*, 2, 457–465. https://doi.org/10.1016/j.redox.2013.12.020

Hanks, J. H. (1975). Hanks' balanced salt solution and pH control. *TCA Manual/Tissue Culture Association*, 1(1), 3–4. https://doi.org/10.1007/BF00914425

Heiken, G., Vaniman, D., & French, B. M. (1991). *Lunar sourcebook: A user's guide to the moon*. Cambridge University Press.

Hendrix, D. A. (2022). *Reactive oxygen species (ROS) generation of minerals analogous to lunar dust and the link to potential human health risks of lunar activities*. State University of New York at Stony Brook.

Hendrix, D. A., Hurowitz, J. A., Glotch, T. D., & Schoonen, M. A. A. (2021). Olivine dissolution in simulated lung and gastric fluid as an analog to the behavior of lunar particulate matter inside the human respiratory and gastrointestinal systems. *GeoHealth*, 5(11), e2021GH000491. https://doi.org/10.1029/2021gh000491

Hendrix, D. A., Port, S. T., Hurowitz, J. A., & Schoonen, M. A. (2019). Measurement of OH* generation by pulverized minerals using electron spin resonance spectroscopy and implications for the reactivity of planetary regolith. *GeoHealth*, *3*(1), 28–42. https://doi.org/10.1029/2018gh000175

Hessel, P., Sluis-Cremer, G., Hnizdo, E., Faure, M., Thomas, R. G., & Wiles, F. (1988). Progression of silicosis in relation to silica dust exposure. In *Inhaled particles VI* (pp. 689–696). Elsevier.

Hnizdo, E., Murray, J., & Klempman, S. (1997). Lung cancer in relation to exposure to silica dust, silicosis and uranium production in South African gold miners. *Thorax*, *52*(3), 271–275. https://doi.org/10.1136/thx.52.3.271

Hnizdo, E., & Vallyathan, V. (2003). Chronic obstructive pulmonary disease due to occupational exposure to silica dust: A review of epidemiological and pathological evidence. *Occupational and Environmental Medicine*, *60*(4), 237–243. https://doi.org/10.1136/oem.60.4.237

Hsu, H. T., Tseng, Y. T., Wong, W. J., Liu, C. M., & Lo, Y. C. (2018). Resveratrol prevents nanoparticles-induced inflammation and oxidative stress via downregulation of PKC-alpha and NADPH oxidase in lung epithelial A549 cells. *BMC Complementary and Alternative Medicine*, *18*(1), 211. https://doi.org/10.1186/s12906-018-2278-6

Hu, G., Cun, X., Ruan, S., Shi, K., Wang, Y., Kuang, Q., et al. (2016). Utilizing G2/M retention effect to enhance tumor accumulation of active targeting nanoparticles. *Scientific Reports*, *6*(1), 27669. https://doi.org/10.1038/srep27669

James, J. T., & Kahn-Mayberry, N. (2009). Risk of adverse health effects from lunar dust exposure. In *The human research program evidence book* NASA-SP-2009-3045 (pp. 317–330). NASA.

Kowaltowski, A. J., de Souza-Pinto, N. C., Castilho, R. F., & Vercesi, A. E. (2009). Mitochondria and reactive oxygen species. *Free Radical Biology and Medicine*, *47*(4), 333–343. https://doi.org/10.1016/j.freeradbiomed.2009.05.004

Kuznetsov, I. A., Zakharov, A. V., Dolnikov, G. G., Lyash, A. N., Afonin, V. V., Popel, S. I., et al. (2017). Lunar dust: Properties and investigation techniques. *Solar System Research*, *51*(7), 611–622. https://doi.org/10.1134/s0038094617070097

Lam, C. W., Castranova, V., Zeidler-Erdely, P. C., Renne, R., Hunter, R., McCluskey, R., et al. (2022). Comparative pulmonary toxicities of lunar dusts and terrestrial dusts (TiO_2 & SiO_2) in rats and an assessment of the impact of particle-generated oxidants on the dusts' toxicities. *Inhalation Toxicology*, *34*(3–4), 51–67. https://doi.org/10.1080/08958378.2022.2038736

Linnarsson, D., Carpenter, J., Fubini, B., Gerde, P., Karlsson, L. L., Loftus, D. J., et al. (2012). Toxicity of lunar dust. *Planetary and Space Science*, *74*(1), 57–71. https://doi.org/10.1016/j.pss.2012.05.023

Loftus, D. J., Tranfield, E. M., Rask, J. C., & McCrosssin, C. (2008). *The chemical reactivity of lunar dust relevant to human exploration of the Moon* (pp. 2–4). NASA Ames Research Center.

Long-Fox, J. M., Landsman, Z. A., Easter, P. B., Millwater, C. A., & Britt, D. T. (2023). Geomechanical properties of lunar regolith simulants LHS-1 and LMS-1. *Advances in Space Research*, *71*(12), 5400–5412. https://doi.org/10.1016/j.asr.2023.02.034

Medina-Reyes, E. I., Bucio-Lopez, L., Freyre-Fonseca, V., Sanchez-Perez, Y., Garcia-Cuellar, C. M., Morales-Barcenas, R., et al. (2015). Cell cycle synchronization reveals greater G2/M-phase accumulation of lung epithelial cells exposed to titanium dioxide nanoparticles. *Environmental Science and Pollution Research International*, *22*(5), 3976–3982. https://doi.org/10.1007/s11356-014-3871-y

Meindl, C., Ohlinger, K., Zrim, V., Steinkogler, T., & Frohlich, E. (2021). Screening for effects of inhaled nanoparticles in cell culture models for prolonged exposure. *Nanomaterials*, *11*(3), 606. https://doi.org/10.3390/nano11030606

Merget, R., Bauer, T., Kupper, H. U., Philippou, S., Bauer, H. D., Breitstadt, R., & Bruening, T. (2002). Health hazards due to the inhalation of amorphous silica. *Archives of Toxicology*, *75*(11–12), 625–634. https://doi.org/10.1007/s002040100266

Mitsopoulos, P., & Suntres, Z. E. (2011). Protective effects of liposomal N-acetylcysteine against paraquat-induced cytotoxicity and gene expression. *Journal of Toxicology*, *2011*, 808967. https://doi.org/10.1155/2011/808967

Mittal, M., Siddiqui, M. R., Tran, K., Reddy, S. P., & Malik, A. B. (2014). Reactive oxygen species in inflammation and tissue injury. *Antioxidants and Redox Signaling*, *20*(7), 1126–1167. https://doi.org/10.1089/ars.2012.5149

Muruzabal, D., Collins, A., & Azqueta, A. (2021). The enzyme-modified comet assay: Past, present and future. *Food and Chemical Toxicology*, *147*, 111865. https://doi.org/10.1016/j.fct.2020.111865

Nowsheen, S., Xia, F., & Yang, E. S. (2012). Assaying DNA damage in hippocampal neurons using the comet assay. *Journal of Visualized Experiments*, *70*, e50049. https://doi.org/10.3791/50049-v

Ovrevik, J., Låg, M., Hetland, R., Schwarze, P., & Refsnes, M. (2002). Stone particle-induced interleukin-6 and -8 release involves activation of MAP kinases and tyrosine kinases. *Annals of Occupational Hygiene*, *46*, 390–392.

Pohlen, M., Carroll, D., Prisk, G. K., & Sawyer, A. J. (2022). Overview of lunar dust toxicity risk. *npj Microgravity*, *8*(1), 55. https://doi.org/10.1038/s41526-022-00244-1

Ryter, S. W., Kim, H. P., Hoetzel, A., Park, J. W., Nakahira, K., Wang, X., & Choi, A. M. (2007). Mechanisms of cell death in oxidative stress. *Antioxidants and Redox Signaling*, *9*(1), 49–89. https://doi.org/10.1089/ars.2007.9.49

Saraf, A., Larsson, L., Larsson, B. M., Larsson, K., & Palmberg, L. (1999). House dust induces IL-6 and IL-8 response in A549 epithelial cells. *Indoor Air*, *9*(4), 219–225. https://doi.org/10.1111/j.1600-0668.1999.00002.x

Skocaj, M., Filipic, M., Petkovic, J., & Novak, S. (2011). Titanium dioxide in our everyday life; is it safe? *Radiology and Oncology*, *45*(4), 227. https://doi.org/10.2478/v10019-011-0037-0

Skuland, T., Lag, M., Gutleb, A. C., Brinchmann, B. C., Serchi, T., Ovrevik, J., et al. (2020). Pro-inflammatory effects of crystalline- and nano-sized non-crystalline silica particles in a 3D alveolar model. *Particle and Fibre Toxicology*, *17*(1), 13. https://doi.org/10.1186/s12989-020-00345-3

Strober, W. (2001). Trypan blue exclusion test of cell viability. *Current Protocols in Immunology*, *21*(1). https://doi.org/10.1002/0471142735.ima03bs21

Tice, R. R., Agurell, E., Anderson, D., Burlinson, B., Hartmann, A., Kobayashi, H., et al. (2000). Single cell gel/comet assay: Guidelines for in vitro and in vivo genetic toxicology testing. *Environmental and Molecular Mutagenesis*, *35*(3), 206–221. https://doi.org/10.1002/(sici)1098-2280(2000)35:3<206::aid-em8>3.0.co;2-j

Van Houten, B., Hunter, S. E., & Meyer, J. N. (2016). Mitochondrial DNA damage induced autophagy, cell death, and disease. *Frontiers in Bioscience*, *21*(1), 42–54. https://doi.org/10.2741/4375

Wagner, S. A. (2006). *The Apollo experience lessons learned for constellation lunar dust management*. NASA Technical Publication TP-2006-213726. National Aeronautics and Space Administration.

Winterhalter, D., Levine, J. S., Kerschmann, R. L., & Brady, T. K. (2020). Lunar dust and its impact on human exploration: A NASA Engineering and Safety Center (NESC) workshop.

Wojtala, A., Bonora, M., Malinska, D., Pinton, P., Duszynski, J., & Wieckowski, M. R. (2014). Methods to monitor ROS production by fluorescence microscopy and fluorometry. *Methods in Enzymology*, *542*, 243–262. Retrieved from https://www.ncbi.nlm.nih.gov/pubmed/24862270

Xu, C., Zhang, M., Chen, W., Jiang, L., Chen, C., & Qin, J. (2020). Assessment of air pollutant $PM_{2.5}$ pulmonary exposure using a 3D lung-on-chip model. *ACS Biomaterials Science & Engineering*, *6*(5), 3081–3090. https://doi.org/10.1021/acsbiomaterials.0c00221

Zhang, M., Xu, C., Jiang, L., & Qin, J. (2018). A 3D human lung-on-a-chip model for nanotoxicity testing. *Toxicology Research*, *7*(6), 1048–1060. https://doi.org/10.1039/c8tx00156a